Rotating magnetic field current drive in a hollow plasma column with a steady toroidal field

Ricardo Farengo and Roberto A. Clemente

Rotating magnetic field current drive in a hollow plasma column with a steady toroidal field

Ricardo Farengo[a]
Centro Atómico Bariloche e Instituto Balseiro, S. C. de Bariloche 8400, R. N. Argentina

Roberto A. Clemente
Instituto de Fisica Gleb Wataghin, Universidade Estadual de Campinas, 13083-970, Campinas, SP, Brazil

The effect of a steady azimuthal magnetic field on rotating magnetic field current drive is studied. The configuration considered consists of an infinitely long plasma column with a finite radius conductor, which carries a steady longitudinal current, running along its axis. The ions are assumed to be fixed and the electrons are described using an Ohm's law that contains the Hall term. A fully two-dimensional computer code is developed to solve the resulting time-dependent equations. For some values of the steady azimuthal field, two steady-state solutions with different efficiencies are found. © *2001 American Institute of Physics.* [DOI: 10.1063/1.1343509]

I. INTRODUCTION

Rotating magnetic fields (RMFs) have been used to drive current in rotamaks[1] and field-reversed configurations (FRCs).[2] Although these devices generally operate without a stationary azimuthal (toroidal) magnetic field, some rotamak experiments included a conductor at the axis of the discharge vessel,[3] producing configurations which are similar to spherical tokamaks (STs). Due to the current interest in STs, which has prompted the construction of several new devices,[4–6] the development of RMF current drive as an efficient method for this concept would be of great importance.

Theoretical studies of RMF current drive have generally considered fixed ions and employed Ohm's law, with the Hall term, to describe the electrons. In configurations without a steady toroidal magnetic field, both stationary and time dependent solutions [in two dimensions (2D)] have been obtained.[7] For these configurations, the effect of anisotropic resistivity and finite radius RMF coils has been also studied.[8] Theoretical studies in configurations with a steady toroidal field have been limited to the calculation of steady state solutions for cylindrical plasma columns having an infinitely thin wire that carries a steady longitudinal current along the symmetry axis.[9,10] These studies assumed that, in steady state, the time-dependent part of all physical quantities can be represented using only the first Fourier harmonic [$\exp\{i(\theta - \omega t)\}$, where ω is the frequency of the rotating magnetic field]. Solving the resulting set of nonlinear equations, which depends on a limited number of parameters such as resistivity, driving magnetic field, and external longitudinal current, Bertram[9] and Watterson[10] showed the possibility of driving a significant amount of current in the azimuthal direction.

Most previous theoretical studies of RMF current drive, both in configurations with and without a steady toroidal field, considered an infinitely long plasma column ($\partial/\partial z \equiv 0$) and employed cylindrical coordinates. For simplicity,

and to be able to compare with previous results, we use a similar geometry and the same coordinates system. However, unlike Refs. 9 and 10, we introduce a finite radius conductor at the center of the plasma column. This eliminates the singularity in the toroidal field at $r = 0$ and allows for the use of boundary conditions which are similar to those corresponding to a tokamak at the inner plasma interface. We use the same physical model as in most previous theoretical studies, fixed ions and Ohm's law with the Hall term for the electrons, but employ a fully two-dimensional (r, θ) numerical code to solve the time-dependent problem. The same nondimensional parameters employed by Milroy,[8] plus the normalized steady toroidal field, are used. These parameters can be easily related to those employed by Watterson.[10]

The structure of this paper is as follows. In Sec. II we present the physical model employed and derive the basic equations describing the evolution of the z components of the magnetic field and vector potential inside the plasma. In Sec. III we describe the numerical methods and boundary conditions used and in Sec. IV the results are presented. Finally, in Sec. V, we summarize and discuss our findings.

II. PHYSICAL MODEL AND ASSUMPTIONS

We consider the configuration shown in Fig. 1. The infinitely long ($\partial/\partial z \equiv 0$) annular plasma column has inner radius r_a and outer radius r_b (zone II). Inside the column (zone I, $r < r_a$) there is a uniform, stationary, axial current density that produces the *vacuum* toroidal field. The coils that produce the transverse, rotating magnetic field are assumed to be far from the plasma and their effect is introduced via the boundary conditions imposed at r_c (zone III: $r_b < r < r_c$, $r_c \gg r_b$). The ions are considered to be fixed, the density of both species is assumed to be equal and uniform, and electron inertia is neglected. Using the following Ohm's law, which contains the Hall term but not the electron pressure gradient:

$$\mathbf{E} = \eta \mathbf{j} + \frac{1}{en}(\mathbf{j} \times \mathbf{B}),$$

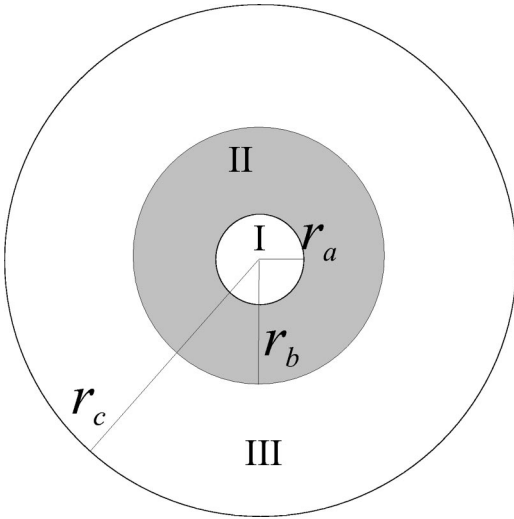[a]Electronic mail: farengo@cab.cnea.gov.ar

FIG. 1. Cross section of the configuration employed.

where η is the plasma resistivity (assumed uniform) and n the density, and Maxwell's equations, a set of coupled equations for the z components of the magnetic field (B_z) and vector potential (A_z, $\mathbf{B} = \nabla \times \mathbf{A}$) can be obtained. Since the contribution of the uniform axial current to A_z can be calculated analytically, we separate A_z in two parts:

$$A_z = A_{z,\text{vac}} + A_{z,\text{pl}}, \tag{1}$$

where $A_{z,\text{vac}}$ contains the contribution of the stationary axial current and $A_{z,\text{pl}}$ the contribution of the plasma and the external coils. Assuming that the rotating magnetic field produced by the coils can be written as

$$B_r^{\text{rot}} = -B_\omega \cos(\omega t - \theta), \tag{2a}$$

$$B_\theta^{\text{rot}} = -B_\omega \sin(\omega t - \theta), \tag{2b}$$

and normalizing the time with ω, the radius with r_b, and the amplitude of the magnetic field with B_ω, we obtain the following set of dimensionless equations:

$$\frac{\partial B}{\partial \tau} = \frac{1}{2\lambda^2} \left\{ \nabla^2 B + \frac{\gamma}{\hat{r}} \left[\frac{\partial}{\partial \hat{r}} (\nabla^2 A) \frac{\partial A}{\partial \theta} \right. \right.$$
$$\left. \left. - \frac{\partial}{\partial \theta} (\nabla^2 A) \left(\frac{\partial A}{\partial \hat{r}} - \frac{B_{\text{tor}}}{\hat{r}} \right) \right] \right\}, \tag{3a}$$

$$\frac{\partial A}{\partial \tau} = \frac{1}{2\lambda^2} \left\{ \nabla^2 A + \frac{\gamma}{\hat{r}} \left[\left(\frac{\partial A}{\partial \hat{r}} - \frac{B_{\text{tor}}}{\hat{r}} \right) \frac{\partial B}{\partial \theta} - \frac{\partial A}{\partial \theta} \frac{\partial B}{\partial \hat{r}} \right] \right\}, \tag{3b}$$

where

$$\hat{r} = \frac{r}{r_b}, \quad \tau = \omega t, \quad B = \frac{B_z}{B_\omega}, \quad A = \frac{A_{z,\text{pl}}}{B_\omega r_b},$$

and B_{tor} is the vacuum toroidal field at $\hat{r} = 1$, normalized to B_ω. The two dimensionless parameters γ and λ are defined as

$$\lambda = \frac{r_b}{\delta} = r_b \left(\frac{\mu_0 \omega}{2\eta} \right)^{1/2}, \quad \gamma = \frac{\Omega_{\omega,e}}{\nu_{e,i}} = \frac{B_\omega}{en\eta},$$

where δ is the classical skin depth, $\Omega_{\omega,e}$ is the electron cyclotron frequency calculated with the amplitude of the RMF, and $\nu_{e,i}$ is the electron–ion collision frequency ($\nu_{e,i} = \eta n e^2 / m_e$). When $\gamma \gg 1$, the electrons can be considered magnetized by the RMF. Knowing A and B, the other magnetic-field components and the current density can be easily calculated.

III. NUMERICAL METHODS AND BOUNDARY CONDITIONS

Previous numerical calculations in configurations without a steady toroidal field generally employed a Fourier expansion in θ (and in most cases used just a few harmonics).[7,8] We will show later that when a steady toroidal field is present there could be a strong θ dependence that makes the use of such expansions less attractive. We developed a fully 2D (r, θ) finite differences code that employs a second-order Runge–Kutta scheme to advance the equations in time. The computational domain is divided in three regions, which generally have different grid spacing in the radial direction. In $0 \leq \hat{r} < \hat{r}_a$, region I, there is a uniform axial current and no plasma. Since A contains only the contribution of the plasma and the RMF coils, and the contribution of the axial current is calculated analytically, we have

$$\nabla^2 A = 0, \quad \hat{r} < \hat{r}_a. \tag{4}$$

Since there are no azimuthal or radial currents in this region, B must be uniform (but can be time dependent)

$$\frac{\partial B}{\partial \hat{r}} = \frac{\partial B}{\partial \theta} \equiv 0.$$

Inside the plasma, $\hat{r}_a < \hat{r} < 1$, region II, we solve Eqs. (3). In $1 < \hat{r} < \hat{r}_c$, region III, there is vacuum and, therefore, B is uniform and A satisfies

$$\nabla^2 A = 0, \quad 1 < \hat{r} < \hat{r}_c. \tag{5}$$

Equations (4) and (5) are solved by inverting the sparse matrices obtained when Laplace's equation is written in finite differences. In Eq. (4), the point $\hat{r} = 0$ is treated separately using local Cartesian coordinates to avoid the divergence of the cylindrical Laplacian operator. It is important to note that for each run of the code the matrix inversion needs to be done only once.

We now discuss the boundary conditions used to solve Eqs. (3), (4), and (5) and the methods employed to calculate B in regions I and III. At $\hat{r} = \hat{r}_c$, we set

$$A(\hat{r}_c) = \hat{r}_c \sin(\tau - \theta)(1 - e^{-\tau/\tau_0}), \tag{6}$$

where the exponential is introduced to allow for a slow ''turn on'' of the rotating field, as done by Hugrass,[7] and $\hat{r}_c$ is taken large enough for the results to be independent of its specific value. The values generally used for τ_0 and $\hat{r}_c$ are, respectively, 0.33 and 5. The value of τ_0 is always much smaller than the time needed to reach steady state and, hence, it does not affect the results. The value of $\hat{r}_c$ is chosen so that any additional increase produces negligible changes in the

results. The boundary condition introduced with Eq. (6) basically means that the coils which produce the RMF have an infinite radius and was employed for simplicity. At $\hat{r}=1$ and $\hat{r}=\hat{r}_a$, the radial derivative of A must be continuous ($B_\theta = -\partial A_z/\partial r$), hence,

$$\left(\frac{\partial A}{\partial \hat{r}}\right)_{1^+} = \left(\frac{\partial A}{\partial \hat{r}}\right)_{1^-} \quad \text{and} \quad \left(\frac{\partial A}{\partial \hat{r}}\right)_{\hat{r}_a^+} = \left(\frac{\partial A}{\partial \hat{r}}\right)_{\hat{r}_a^-}.$$

To obtain the results presented below, the value of B in region III was kept constant throughout the computation but it is also possible to introduce a flux conserver and adjust B after each time step to satisfy axial flux conservation. The exact value given to B in this region is not relevant because Eq. (3) only contains derivatives of B. In region I, B is uniform but not constant (in time) and we calculate its value using Stokes' theorem. Considering a circumference of radius $\hat{r}_a+h$, where h is the radial grid spacing in region II, we can write

$$\int_0^{2\pi} A_\theta(\hat{r}_a+h,\theta)\hat{r}\,d\theta = \int_0^{\hat{r}_a+h} d\hat{r}\hat{r}\int_0^{2\pi} d\theta B(\hat{r},\theta),$$

where A_θ is also normalized with $B_\omega r_b$. Since B is uniform inside the circle of radius $\hat{r}_a$, we can write

$$B(I) \equiv B(\hat{r}_a) = \frac{1}{\pi\hat{r}_a^2}\left\{\int_0^{2\pi} A_\theta(\hat{r}_a+h,\theta)\hat{r}\,d\theta \right.$$

$$\left. - \int_{\hat{r}_a}^{\hat{r}_a+h} d\hat{r}\hat{r}\int_0^{2\pi} d\theta B(\hat{r},\theta)\right\}. \qquad (7)$$

Equation (7) shows that to calculate $B(I)$ we need $B(II)$, which is given by Eq. (3) and $A_\theta(\hat{r}_a+h,\theta)$. The equation for the evolution of A_θ in region II is obtained from the θ component of Ohm's law, using $\mathbf{E} = -\partial\mathbf{A}/\partial t$, and can be written in dimensionless form as

$$\frac{\partial A_\theta}{\partial \tau} = \frac{1}{2\lambda^2}\left\{\frac{\partial B}{\partial \hat{r}} + \frac{\gamma}{\hat{r}}\left[\left(\frac{\partial A}{\partial \hat{r}} - \frac{B_{\text{tor}}}{\hat{r}} + \hat{r}\left[\frac{\partial^2 A}{\partial \hat{r}^2} + \frac{B_{\text{tor}}}{\hat{r}^2}\right] + \frac{1}{\hat{r}}\frac{\partial^2 A}{\partial\theta^2}\right)\right.\right.$$

$$\left.\left. \times\frac{1}{\hat{r}}\frac{\partial A}{\partial\theta} + B\frac{\partial B}{\partial\theta}\right]\right\}. \qquad (8)$$

It can be seen that we only need A and B in region II to advance $A_\theta(r_a+h,\theta)$ in time and calculate $B(I)$.

The numerical algorithm employed is as follows:

(1) The values of the basic dimensionless parameters, B_{tor}, λ, and γ, are fixed and the initial values of A, B, and A_θ are defined. In general, the same value is given to B at all grid points and A is set equal to zero in regions I and II. In region III, A is defined as

$$A = -\frac{\Delta\tau}{\tau_0}\sin(\theta)\left(\hat{r} - \frac{1}{\hat{r}}\right),$$

where $\Delta\tau$ is the time step. This is a solution to Laplace's equation in region III, which is consistent for large values of $\hat{r}_c$ and short times with the boundary condition introduced in Eq. (6). Since B is

defined to be the same everywhere, $A_\theta(r+h,\theta)$ does not depend on θ and can be calculated from

$$2\pi(r+h)A_\theta(r+h) = \pi(r+h)^2 B.$$

(2) The inverse matrices of Eqs. (4) and (5) are calculated.

(3) $B(\hat{r}_a)$ is calculated using Eq. (7) and the values of $A_\theta(\hat{r}_a+h,\theta)$ and $B(II)$ obtained in the previous time step. $A(\hat{r}_c)$ is calculated using Eq. (6). Of course, this is not necessary for the first time step where the initial values are employed.

(4) $A(\hat{r}_a)$ and $A(1)$ are calculated. This is done using the following procedure:

  (a) Using the values of A inside region II, from $\hat{r}_a+h$ to $1-h$, estimates for $A(\hat{r}_a)$ and $A(1)$ are obtained.

  (b) Using these estimates as boundary values, Eqs. (4) and (5) are solved.

  (c) Using the values of $A(\hat{r}_a-h)$ and $A(1+h)$ calculated with Eqs. (4) and (5), *new* values of $A(\hat{r}_a)$ and $A(1)$ are defined as

$$A^{\text{new}}(\hat{r}_a) = \tfrac{1}{2}[A(\hat{r}_a-h)+A(\hat{r}_a+h)],$$

$$A^{\text{new}}(1) = \tfrac{1}{2}[A(1-h)+A(1+h)].$$

  (d) The new values are compared with the old ones. If the relative difference between the two values is less than a small quantity (typically, 10^{-3}–10^{-4}), the values are accepted, otherwise the new values are used as boundary conditions to solve Eqs. (4) and (5) and the procedure is repeated until convergence is achieved.

(5) Equations (3) and (8) are advanced in time using the boundary conditions defined above. A small time step, $\Delta\tau = (\pi/4)\times10^{-4}$, was employed to obtain the results presented below.

Steps (3)–(5) are repeated until the equations are advanced up to the desired time. The code can also be started by initializing A, B, and A_θ with any previous solution.

IV. RESULTS

Unless otherwise indicated, normalized quantities are employed in the plots presented below. The current density is normalized to $B_\omega/\mu_0 r_b$ and the efficiency is defined as the ratio between the azimuthal plasma current and the current that would be produced if all the electrons rotate rigidly with frequency ω:

$$\alpha = \frac{2[B_z(r_b) - B_z(r_a)]}{\mu_0 n e \omega(r_b^2 - r_a^2)}.$$

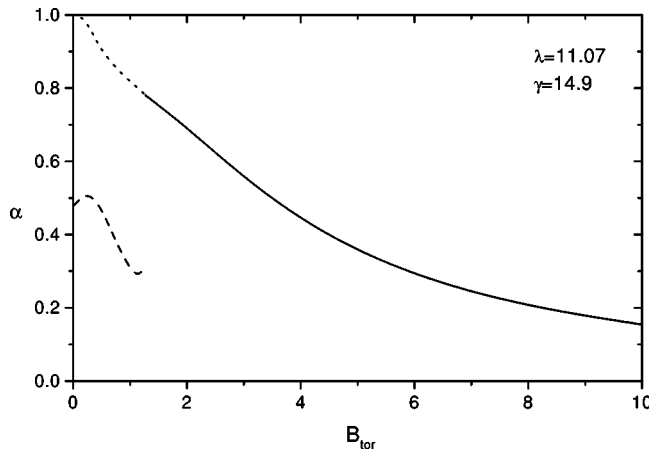To compare with existing results for configurations without a steady toroidal field (FRC), we use the same values of λ and

FIG. 2. Efficiency vs steady toroidal field for $\gamma = 14.9$, $\lambda = 11.07$, and $\hat{r}_a = 0.15$.

FIG. 3. Efficiency vs steady toroidal field for $\gamma = 16.6$, $\lambda = 11.07$, and $\hat{r}_a = 0.15$.

γ as in Ref. 8, where they were chosen to be representative of the Star Thruster Experiment.[2]

Hugrass[11] first reported, in configurations without a steady toroidal field, that there are nonunique steady state solutions when $\lambda \gtrsim 6$ and $\gamma \approx \lambda$. As noted by Milroy,[8] this is due to the existence of hysteresis. When γ is increased, the RMF does not penetrate completely until a critical value is exceeded. However, once full penetration has been achieved, γ can be reduced significantly below this critical value before the RMF is expelled, and the efficiency reduced. A similar effect is shown in Fig. 2, which presents a plot of the steady state efficiency as a function of the normalized, steady, toroidal field (B_{tor}) for $\gamma = 14.9$, $\lambda = 11.07$, and $\hat{r}_a = 0.15$ [aspect ratio $A = (1 + \hat{r}_a)/(1 - \hat{r}_a) = 1.35$]. When $B_{tor} = 0$, and a plasma column that has no azimuthal current is used as initial condition, the steady state efficiency obtained is $\alpha = 0.48$. This value is similar, but not equal, to the value obtained for a FRC for the same values of γ and λ ($\alpha = 0.42$).[8] The small difference could be due to the different geometry (we are considering a hollow plasma column) and, in part, to the different numerical methods employed. As B_{tor} is increased, the solution follows the low efficiency branch (dashed line in Fig. 2) until B_{tor} reaches a critical value ($B_{tor}^{crit} \cong 1.26$). When B_{tor} becomes larger than the critical value the efficiency of the steady state solution *jumps* to the full line in Fig. 2 and follows this line as B_{tor} is increased further. However, when B_{tor} is reduced, the steady state solution follows the high efficiency branch (dotted line in Fig. 2), and a solution with efficiency equal to 1 is obtained for $B_{tor} = 0$. This solution can be also obtained starting with $\gamma = 16.6$ and $B_{tor} = 0$ (see below) and slowly decreasing γ.

We note that in the low efficiency branch the efficiency initially increases when B_{tor} increases and later decreases. This behavior was observed in the experiments[3] and also reported in Refs. 9 and 10. Another important remark regarding Fig. 2 is that although the efficiency decreases as B_{tor} increases (in the high efficiency branch), the larger radius of a tokamak, compared with a FRC, could partially compensate for this reduction. Figure 3 presents a similar plot for $\gamma = 16.6$ and the same values of λ and $\hat{r}_a$ as in Fig. 2. The
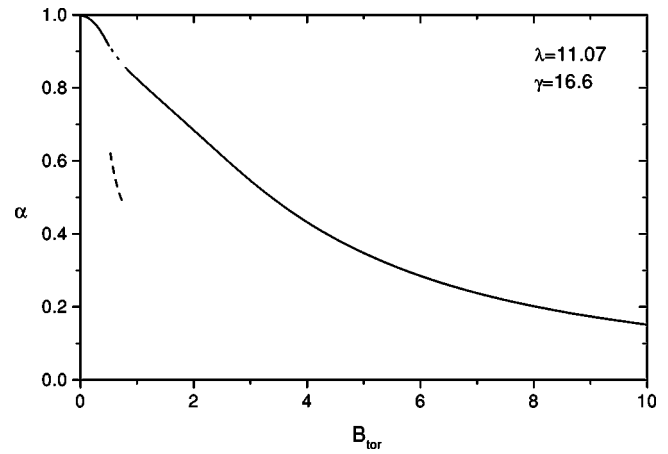
efficiency obtained in this case for $B_{tor} = 0$ ($\alpha = 1$) agrees with the value obtained for a FRC.[8] Two solutions can be observed for $0.53 \leqslant B_{tor} \leqslant 0.77$. As in Fig. 2, the initial conditions determine the branch towards which the plasma evolves. Starting with a plasma without azimuthal current, the solution falls in the high efficiency branch (full line) when $0 \leqslant B_{tor} \leqslant 0.53$, in the low efficiency branch (dashed line) when $0.53 < B_{tor} \leqslant 0.77$, and back into the high efficiency branch when $B_{tor} > 0.77$. To obtain a high efficiency steady state solution with $0.53 \leqslant B_{tor} \leqslant 0.77$ (dotted line), it is necessary to start with a high efficiency solution having B_{tor} greater than 0.77 (smaller than 0.53) and slowly decrease (increase) B_{tor}. The two high efficiency and the two low efficiency solutions of Figs. 2 and 3 display a similar behavior when features such as RMF penetration, diamagnetism, azimuthal current profile, and θ dependence are analyzed. In what follows, we will consider two cases: the low efficiency regime of Fig. 2, with $\gamma = 14.9$, and the high efficiency regime of Fig. 3, with $\gamma = 16.6$.

In Refs. 7 and 8 it is shown that in configurations without a steady toroidal field, there is a direct relationship between the current drive efficiency and the degree of penetration of the RMF. The same experiments[3] that show an initial increase in efficiency as the steady toroidal field increases (see above) also show that RMF penetration continues to improve beyond the value of B_{tor} where the efficiency reaches its maximum value. This behavior is also seen in Fig. 4, which presents a plot of the averaged (over θ) modulus of the transverse field ($B_{tr} = \sqrt{B_r^2 + B_\theta^2}$, where all the components of the magnetic field are normalized to B_ω and B_θ does not include the steady toroidal field component) as a function of radius for three values of B_{tor} for the low efficiency branch of Fig. 2. It is clear that RMF penetration improves as B_{tor} increases. The minima in the curves for $B_{tor} = 0.5$ and $B_{tor} = 1.15$ occur at approximately the same radius where the current density reverses (see below). The effect of the steady toroidal field on RMF penetration for the high efficiency branch of Fig. 3 is shown in Figs. 5(a) and 5(b). Figure 5(a) is a plot of B_{tr} vs $\hat{r}$ for three values of B_{tor} and shows that in this case the transverse field inside the
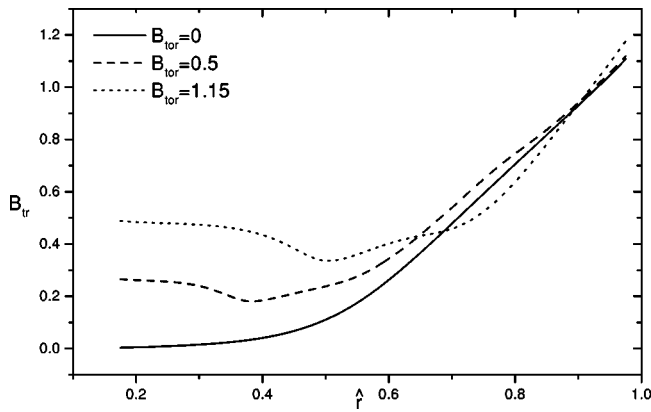
FIG. 4. Modulus of the transverse field (averaged over θ) vs normalized radius for $\gamma = 14.9$, $\lambda = 11.07$, and $\hat{r}_a = 0.15$ (low efficiency branch).

FIG. 6. Current drive efficiency vs normalized time for $\gamma = 14.9$, $\lambda = 11.07$, and $\hat{r}_a = 0.15$ (low efficiency branch).

plasma can be larger than outside, when $B_{tor} \neq 0$, and that its amplitude has a maximum as a function of B_{tor}. This is seen more clearly in Fig. 5(b), which presents a plot of $B_{tr}(\hat{r} = 0.175)$ vs B_{tor} for $\gamma = 16.6$ (high efficiency branch) and the same values of λ, and $\hat{r}_a$ used above.

The dynamics of field penetration and current drive is also affected by the steady toroidal field. This is shown in Figs. 6 and 7, which present plots of the current drive effi-
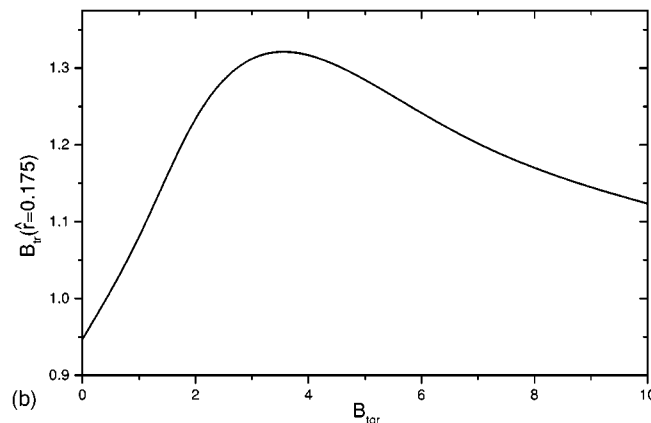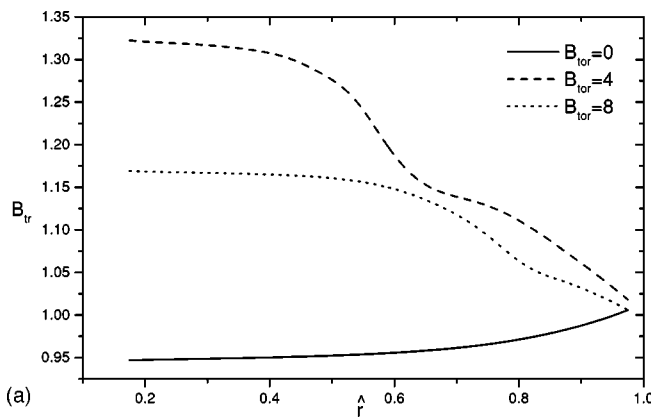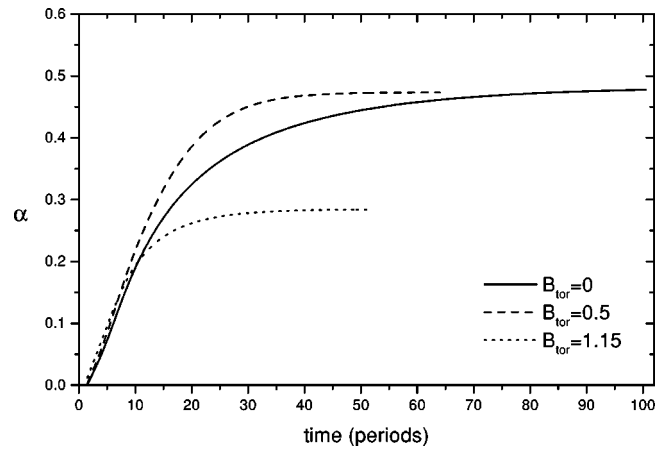
ciency as a function of time for three values of the steady toroidal field. Figure 6 has $\gamma = 14.9$ and corresponds to the low efficiency branch of Fig. 2. Figure 7 has $\gamma = 16.6$ and corresponds to the high efficiency branch of Fig. 3. Figure 6 shows that although the final efficiency varies as B_{tor} increases, the initial slope in the curves of efficiency versus time remains basically unchanged. A different behavior is shown in Fig. 7: when $B_{tor} = 4$, the initial slope is significantly larger and saturation is reached sooner than for $B_{tor} = 0$. When $B_{tor} = 8$ saturation is also reached sooner, but due to the much lower final efficiency the slope is always smaller than for $B_{tor} = 0$.

The effect of the steady toroidal field on the azimuthal current density profile is shown in Figs. 8 and 9. Figure 8 presents a plot of the averaged (over θ) azimuthal current density versus $\hat{r}$ for the low efficiency branch of Fig. 2 and three values of B_{tor}. When $B_{tor} = 0$ (full line) there is a large region, up to $\hat{r} \approx 0.5$, inside the plasma with negligible current density and a narrow region, $\hat{r} \gtrsim 0.9$, on the outside where the electrons rotate rigidly with frequency ω. When $B_{tor} = 0.5$ (dashed line) the current density increases on the inside, in the region $0.3 \lesssim \hat{r} \lesssim 0.5$, and decreases for $\hat{r} \gtrsim 0.6$,

FIG. 5. (a) Modulus of the transverse field (averaged over θ) vs normalized radius for $\gamma = 16.6$, $\lambda = 11.07$, and $\hat{r}_a = 0.15$ (high efficiency branch). (b) Modulus of the transverse field (averaged over θ) at $\hat{r} = 0.175$ vs B_{tor} for $\gamma = 16.6$, $\lambda = 11.07$, and $\hat{r}_a = 0.15$ (high efficiency branch).
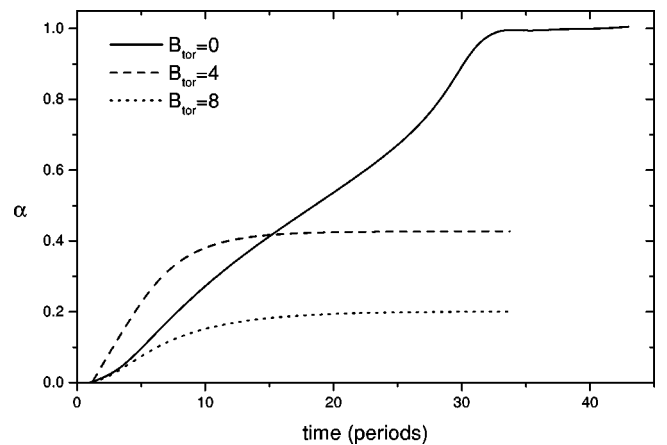

FIG. 7. Current drive efficiency vs normalized time for $\gamma = 16.6$, $\lambda = 11.07$, and $\hat{r}_a = 0.15$ (high efficiency branch).

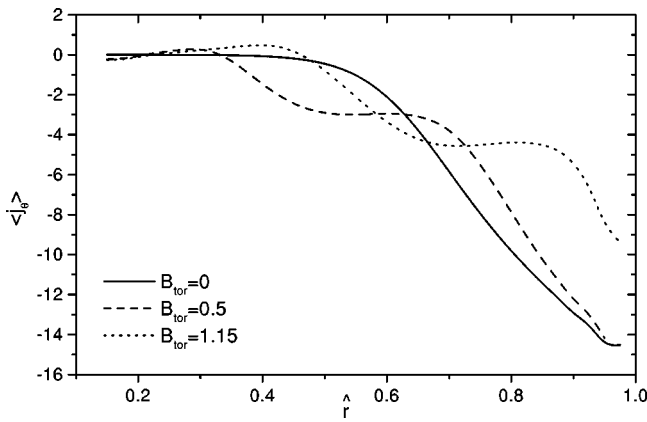FIG. 8. Averaged (over θ) azimuthal current density as a function of normalized radius for $\gamma = 14.9$, $\lambda = 11.07$, and $\hat{r}_a = 0.15$ (low efficiency branch).

FIG. 10. Ratio between the averaged, total, azimuthal field and the vacuum field for $\gamma = 14.9$, $\lambda = 11.07$, and $\hat{r}_a = 0.15$ (low efficiency branch).

giving an overall increase in the total plasma current. Finally, when $B_{tor} = 1.15$, the current density is comparable to that obtained with $B_{tor} = 0$ for $\hat{r} \lesssim 0.6$ and significantly smaller at larger radius. Figure 9 presents a plot of the averaged azimuthal current density versus $\hat{r}$ for the high efficiency branch of Fig. 3 and three values of B_{tor}. When $B_{tor} = 0$ the electrons rotate with frequency ω and the efficiency is 1. As the steady toroidal field increases, a region with negligible, even reversed, current density appears, resulting in a reduction in the total current. As B_{tor} increases further, the width of this region increases.

Experimental measurements in rotamaks with a steady toroidal field[3] and theoretical calculations in infinitely long plasma columns, also with a steady toroidal field,[9,10] have shown the existence of poloidal currents in the former and axial currents in the later, which are generally diamagnetic. We studied this issue for the two conditions indicated above. For the low efficiency regime of Fig. 2 there is a significant diamagnetic effect, which is shown in Fig. 10. This figure presents a plot of the ratio between the averaged (over θ) azimuthal field and the vacuum field as a function of $\hat{r}$. For $B_{tor} = 0.5$ the diamagnetic well extends from $\hat{r} \simeq 0.3$ to the outer plasma boundary, with a maximum reduction in the
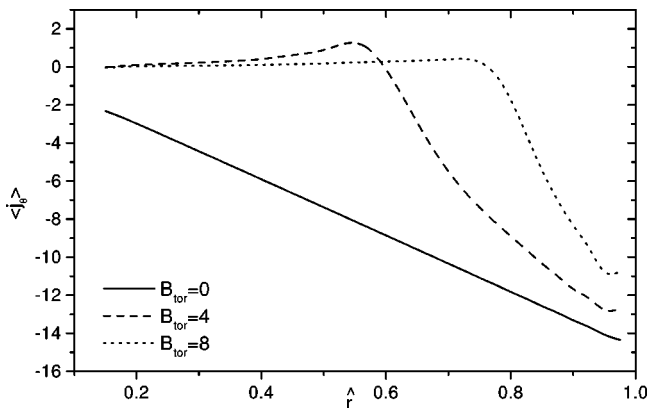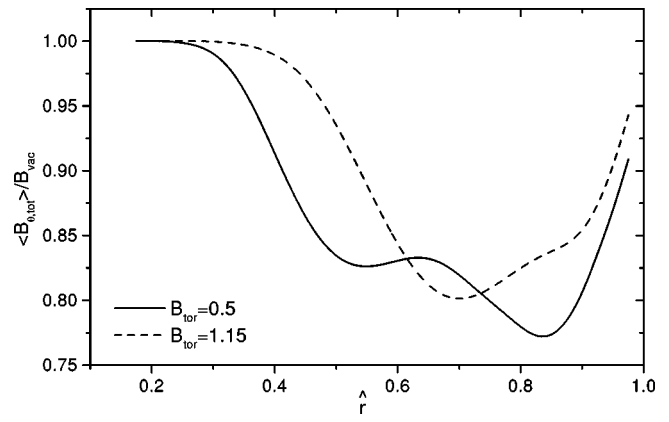
total field of over 20% (compared with the vacuum value). For $B_{tor} = 1.15$ the width and depth of the well decrease but the diamagnetism continues to be significant. For the high efficiency branch of Fig. 3, with $\gamma = 16.6$, the diamagnetism is negligible, as shown in Fig. 11.

Previous theoretical studies in configurations with a steady toroidal field[9,10] assumed that in steady state the time-dependent part of all physical quantities can be described using only the first Fourier harmonic. To check this approximation we investigated the dependence of A and B with respect to $\theta - \tau$, in steady state. In all the cases analyzed the main contribution to the $\theta - \tau$ dependence of A comes from the first harmonic. There are, however, clear differences between the high and low efficiency branches. For the high efficiency branch, the $\theta - \tau$ dependence can be approximated almost exactly using only the first harmonic, while for the low efficiency branch higher-order harmonics also contribute. This can be seen in Fig. 12, which presents plots of $A(\hat{r} = 0.85)$ vs θ (fixed τ, well after a steady state situation has been reached) for two cases: the full line has $B_{tor} = 4$ and $\gamma = 16.6$ and corresponds to the high efficiency branch, and the dashed line has $B_{tor} = 0.5$ and $\gamma = 14.9$ and corresponds to the low efficiency branch. The $\theta - \tau$ dependence of B is similar for the high and low efficiency branches. It varies with
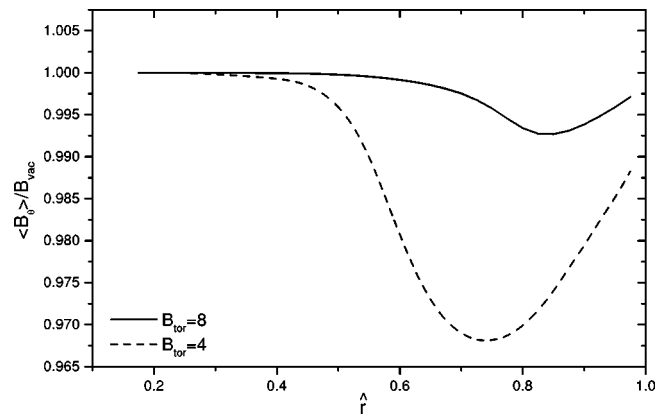

FIG. 9. Averaged (over θ) azimuthal current density as a function of normalized radius for $\gamma = 16.6$, $\lambda = 11.07$, and $\hat{r}_a = 0.15$ (high efficiency branch).

FIG. 11. Ratio between the averaged, total, azimuthal field and the vacuum field for $\gamma = 16.6$, $\lambda = 11.07$, and $\hat{r}_a = 0.15$ (high efficiency branch).
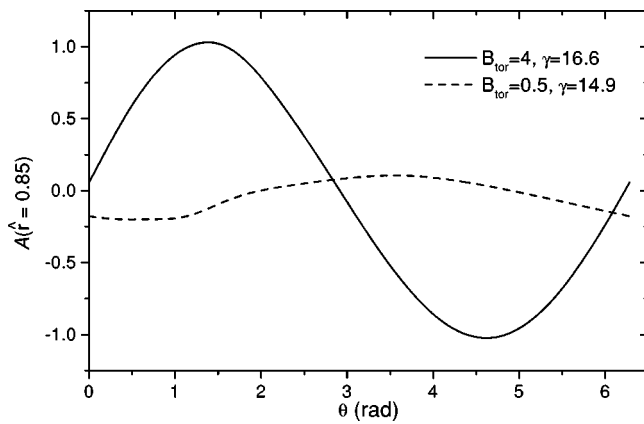
FIG. 12. Azimuthal variation of $A(\hat{r}=0.85)$ for $\lambda=11.07$ and $\hat{r}_a=0.15$. Full line: high efficiency branch ($B_{tor}=4$, $\gamma=16.6$); dashed line: low efficiency branch ($B_{tor}=0.5$, $\gamma=14.9$).

B_{tor} and also with the radial position. When $B_{tor}=0$ there is a gentle oscillation that could be approximated fairly well with a $\cos[2(\theta-\tau)]$ dependence at all radii. This is in agreement with the approximation usually employed in theoretical analysis of RMF current drive in FRCs, where it is assumed that B has only even harmonics. Increasing B_{tor}, a localized maximum which has a large contribution from higher-order harmonics appears at large radius. At small radius, the dependence can be approximated using a simple $\sin(\theta-\tau)$. This can be seen in Fig. 13, which presents a plot of B vs θ (fixed τ) for $B_{tor}=4$ and $\gamma=16.6$ (high efficiency branch) at various radii. The complicated structure of B (and j) implied by Fig. 13 requires further investigations. As expected, exactly the same plots are obtained if we fix θ and vary τ.

V. SUMMARY AND DISCUSSION

As a first step towards assessing the possibility of using RMF current drive in STs, we studied the effect of a steady toroidal field on this method. Our work presents two main improvements when compared to previous studies. The first is the use of a configuration which, albeit 2D, includes a hole
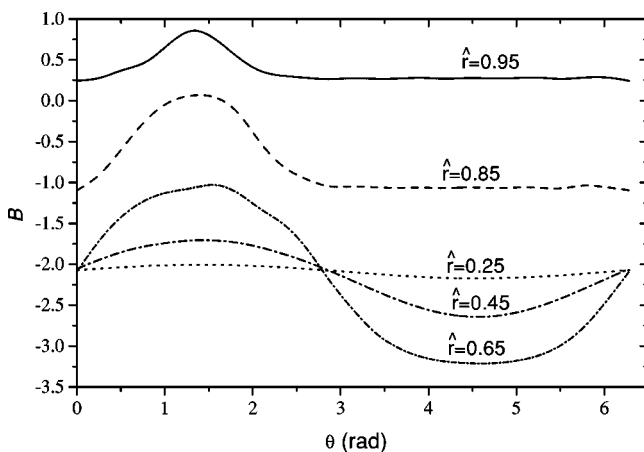
at the center of the plasma, thus providing a better representation of a tokamak. The second is the use of a fully 2D numerical code which solves the time-dependent equations obtained from the basic physical model without further assumptions.

Although we did not attempt to make a detailed comparison with the experimental results of Ref. 3, it is clear that many of the qualitative features observed in these experiments are reproduced by the low efficiency branch of Fig. 2. Our results show that for some values of the external toroidal field, there are two steady state solutions with different efficiencies. When the steady toroidal field is large compared to the rotating field, the case of interest for STs, the efficiency is small but the total current could still be significant if operation at frequencies of the order of 10^6 Hz is possible. Further studies should be done to find the best operating regime for STs and the corresponding efficiency and required power. In addition, two fluid models should be developed to remove some of the most critical assumptions of the present physical model.

After this work was completed, two new papers[12,13] have been published on RMF current drive in FRCs. These papers show that the axial equilibrium condition is a key ingredient to explain important features of the experimental results (i.e., the fact that the RMF penetrates only to the field null[2]). In addition, Ref. 13 uses a magnetohydrodynamics model with finite ion flow, thus removing some of the most critical assumptions of previous studies. Clearly, the importance of these effects in configurations with a steady toroidal field needs to be addressed.

[1] I. R. Jones and W. N. Hugrass, J. Plasma Phys. **26**, 441 (1981).
[2] J. T Slough and K. E. Miller, Phys. Rev. Lett. **85**, 1444 (2000).
[3] G. A. Collins, G. Durance, G. R. Hogg, J. Tendys, and P. A. Watterson, Nucl. Fusion **28**, 255 (1988).
[4] M. Ono, S. M. Kaye, Y.-K. M. Peng, G. Barnes, W. Blanchard, M. D. Carter, J. Chrzanowski, L. Dudek, R. Ewig, D. Gates, R. E. Hatcher, T. Jarboe, S. C. Jardin, D. Johnson, R. Kaita, M. Kalish, C. E. Kessel, H. W. Kugel, R. Maingi, R. Majeski, J. Manickam, G. Oliaro, F. Paollettic, R. Parsells, E. Perry, N. Pomphrey, S. Ramakrishnan, R. Raman, G. Rewoldt, J. Robinson, A. L. Roquemore, P. Ryan, S. Sabbagh, D. Swain, E. J. Synakowski, M. Viola, M. Williams, J. Wilson, and NSTX Team, Nucl. Fusion **40**, 557 (2000).
[5] A. Sykes, *Fusion Energy 1998* (International Atomic Energy Agency, Vienna, 1999), Vol. 1, p. 129.
[6] V. K. Gusev, V. E. Golant, E. Z. Gusakov, V. V. Dyachenko, M. A. Irzak, V. B. Minaev, E. E. Mukhin, A. N. Novokhatskii, K. A. Podushnikova, G. T. Razdobarin, N. V. Sakharov, O. N. Shcherbinin, V. S. Uzlov, V. A. Belyakov, A. A. Kavin, Yu. A. Kostzov, E. G. Kuzmin, V. F. Soikin, E. A. Kuznetzov, V. A. Yagnov, N. Ya Dvorkin, and V. V. Mikov, *Fusion Energy 1998* (International Atomic Energy Agency, Vienna, 1999), Vol. 3, p. 1139.
[7] W. N. Hugrass and R. C. Grimm, J. Plasma Phys. **26**, 455 (1981).
[8] R. D. Milroy, Phys. Plasmas **6**, 2771 (1999).
[9] W. K. Bertram, J. Plasma Phys. **37**, 423 (1987).
[10] P. A. Watterson, J. Plasma Phys. **40**, 109 (1988).
[11] W. N. Hugrass, Aust. J. Phys. **38**, 157 (1985).
[12] A. L. Hoffman, Nucl. Fusion **40**, 1523 (2000).
[13] R. D. Milroy, Phys. Plasmas **7**, 4135 (2000).

FIG. 13. Azimuthal variation of B at various radii for the high efficiency branch with $B_{tor}=4$ ($\gamma=16.6$, $\lambda=11.07$, and $\hat{r}_a=0.15$).